Carbohydrate Polymers 92 (2013) 1783–1791

Contents lists available at SciVerse ScienceDirect

Carbohydrate Polymers

journal homepage: www.elsevier.com/locate/carbpol

Chitosan nanocomposite films: Enhanced electrical conductivity, thermal stability, and mechanical properties

Jason B. Marroquin [a], K.Y. Rhee [a,*], S.J. Park [b,**]

[a] Department of Mechanical Engineering, Kyung Hee University, 446-701, Seoul, Republic of Korea
[b] Department of Chemistry, Inha University, 402-751, Incheon, Republic of Korea

ARTICLE INFO

Article history:
Received 5 September 2012
Received in revised form 31 October 2012
Accepted 8 November 2012
Available online 23 November 2012

Keywords:
Chitosan
Multiwalled carbon nanotubes
Electrical conductivity
Mechanical properties
Nanocomposite
Fe_3O_4

ABSTRACT

A novel, high-performance Fe_3O_4/MWNT/Chitosan nanocomposite has been prepared by a simple solution evaporation method. A significant synergistic effect of Fe_3O_4 and MWNT provided enhanced electrical conductivity, mechanical properties, and thermal stability on the nanocomposites. A 5% (wt) loading of Fe_3O_4/MWNT in the nanocomposite increased conductivity from 5.34×10^{-5} S/m to 1.49×10^{-2} S/m compared to 5% (wt) MWNT loadings. The Fe_3O_4/MWNT/Chitosan films also exhibited increases in tensile strength and modulus of 70% and 155%, respectively. The integral procedure decomposition temperature (IPDT) was enhanced from 501 °C to 568 °C. These effects resulted from a number of factors: generation of a greater number of conductive channels through interactions between MWNT and Fe_3O_4 surfaces, a higher relative crystallinity, the antiplasticizing effects of Fe_3O_4, a restricted mobility and hindrance of depolymerization of the Chitosan chain segments, as well as uniform distribution, improved dispersion, and strong interfacial adhesion between the MWNT and Chitosan matrix.

1. Introduction

Chitosan, the linear and partly acetylated (1–4)-2-amino-2-deoxy-β-D-glucan, is obtained from chitin, the second most abundant natural polymer on earth (Muzzarelli, Boudrant, et al., 2012). It has been investigated extensively over several decades for use in separation membranes, artificial skin, bone substitutes, and water treatment. It possesses a number of interesting properties including biocompatibility, biodegradability, and solubility in aqueous media (Fernandes et al., 2010; Muzzarelli, Greco, Busilacchi, Sollazzo, & Gigante, 2012; Tang et al., 2009; Venkatesan & Kim, 2010). Despite the numerous advantages and unique properties of Chitosan, its poor mechanical and electrical properties restrict its use in a wider range of applications. An effective approach for improving the physical and mechanical properties of Chitosan is to form organic–inorganic composites through incorporation of fillers, such as clays, hydroxyapatite, metal nanoparticles, and carbon nanotubes (Cai et al., 2009; Darder, Colilla, & Ruiz-Hitzky, 2003; Li, Jiang, Huang, Ding, & Chen, 2008; Wang, Shen, Zhang, & Tong, 2005).

Electrically conductive composites with carbon nanotube (CNT) fillers have attracted increasing attention for a variety of applications such as static-charge dissipation (Kwon & Kim, 2005), electromagnetic interference (EMI) shielding (Li et al., 2006) and actuators (Landi et al., 2002). However, CNTs often aggregate in bundles or become entangled because of very strong intertubular van der Waals attractions, which limits their applications (Ajayan, Schadler, Giannaris, & Rubio, 2000). Chemical modification of CNTs has been adopted to improve their interfacial interactions and overall dispersion. However, the atomic structural perfection of CNTs is impaired by chemical modification, which leads to degradation of CNT electrical and mechanical performance (Yao, Yuan, Dang, & Bai, 2010). Chitosan can be made to possess amphiphilic properties that give it a unique capacity to solubilize hydrophobic multiwalled carbon nanotubes (MWNT) in aqueous solution (Liu, Tang, Chen, & Xin, 2005; Tkac, Whittaker, & Ruzgas, 2007; Watts et al., 2001).

Many attempts have been made to improve the biocompatibility and other activities of Chitosan by fabrication of nanocomposites with metal oxide nanoparticles. Due to the magnetic nature of Fe_3O_4, these materials can be used to improve the delivery and recovery of biomolecules for biosensing applications (Miao & Tan, 2000; Xu, Cai, He, & Fang, 2001). In addition, the nanoparticles have a unique ability to promote fast electron transfer between an electrode and the active site of an enzyme, thus further improving their scope as biosensors. Efforts have been made to improve the electrical properties of Chitosan for biosensor applications by the dispersion of superparamagnetic Fe_3O_4 nanoparticles (Kaushik et al., 2008). The adsorption of Chitosan onto Fe_3O_4 has been reported to occur by an electrostatic attraction mechanism (Zhu, Yuan, & Liao, 2008), making Chitosan an effective dispersant

* Corresponding author. Tel.: +82 31 201 2565; fax: +82 31 202 6693.
** Co-corresponding author. Tel.: +82 42 860 7234; fax: +82 42 860 7234.
E-mail addresses: rheeky@khu.ac.kr (K.Y. Rhee), sjpark@inha.ac.kr (S.J. Park).

0144-8617/$ – see front matter © 2012 Elsevier Ltd. All rights reserved.
http://dx.doi.org/10.1016/j.carbpol.2012.11.042

for the preparation of magnetic suspensions stabilized through electrostatic repulsive forces.

Recently, a magnetic solid-phase extraction method was devised, which used magnetic multiwalled carbon nanotubes (mMWNT). These mMWNT were fabricated based on a proposed "aggregation wrap" mechanism that led to the preparation of other self-aggregated magnetic micro/nano carbon materials (Ding et al., 2011). Various methods have been proposed for the preparation of mMWNT, most commonly by assembling magnetic nanoparticles onto MWNT via chemical and/or physical modification. However, most of these methods are complicated and tedious. Furthermore, these modifications may alter the surface chemistry properties as well as other physicochemical properties of MWNT (Georgakilas et al., 2007). Furthermore, a study of the interactions between single walled carbon nanotubes (SWCNTs) and Fe_3O_4 (0 0 1) surfaces by density functional theory (DFT) calculations determined SWCNTs with C vacancies can form chemical bonds with the Fe_3O_4 (0 0 1) surface (Yin et al., 2011). The formation of chemical bonds was found to be critical for promoting electrical conductivity between SWCNTs and transition metal (TM) oxides, suggesting that the use of TM atoms/clusters could be an effective way to enhance the electrical conductivity of electrodes made of mixed SWCNTs and TM oxide nanoparticles. In addition, MWNT/Fe_3O_4 nanoparticle composites, for applications such as electrochemical sensing and solid phase extraction, have been prepared that provided promising properties for the immobilization of substances by electrochemical doping (Yu, Gou, Zhou, Bao, & Gu, 2011). Some studies (Qua, Wang, Kong, Yang, & Chen, 2007) have employed this effect to immobilize glucose oxidase, with the composite magnetically loaded on an electrode with the aid of magnets, as a useful approach to renewable MWNT-based biosensors.

The ability of Chitosan to disperse Fe_3O_4 as well as MWNT and the facile adsorption of Fe_3O_4 by MWNT (Ding et al., 2011; Luo, Yu, Yuan, & Feng, 2012; Yin et al., 2011; Zhao et al., 2011) enables Chitosan to combine the mechanical and electrical properties of MWNT and Fe_3O_4 with the macroporous scaffold forming properties of Chitosan. These Fe_3O_4/MWNT/Chitosan nanocomposites hold promise in providing a breakthrough platform technology for biosensing or bioenergetic applications (Liu et al., 2006; Qian & Yang, 2006; Wescott, Kung, & Maiti, 2007; Zhang, Smith, & Gorski, 2004). Henceforth in this study, in order to expand the various applications of Chitosan, a simple solution evaporation method was used to prepare novel Fe_3O_4/MWNT/Chitosan nanocomposites. The three-component nanocomposite is expected to have diverse properties because each component would contribute different chemical and physical properties. The main objective of this study was to investigate the synergistic effect of Fe_3O_4 and MWNT on the electrical and mechanical properties of Chitosan nanocomposites.

2. Materials and methods

2.1. Reagents and materials

Chitosan (average molecular weight 350 kDa, 90% degree of deacetylation) was purchased from Sigma–Aldrich. Raw multiwalled carbon nanotubes (MWNT, Product No. CM-95), synthesized via the chemical vapor deposition (CVD) method, were purchased from Hanhwa Nanotech Co. Ltd., Korea. The MWNT had diameters of 10–15 nm, tube lengths of 10–20 μm, and a purity of 95%. Magnetite (Fe_3O_4) nanopowder, (<50 nm particle size (TEM), ≥98% trace metals basis) was purchased from Sigma–Aldrich. Acetic acid was used to dissolve Chitosan in distilled water.

2.2. Preparation of nanocomposite films

The complete process for nanocomposite preparation is presented in Scheme 1. Chitosan nanocomposite films containing Fe_3O_4 and MWNT were prepared by a simple solution mixing-evaporation method (Wang, Shen, Zhang, et al., 2005). The concentrations of functional additives (Fe_3O_4 and MWNT) were varied in order to evaluate synergistic effects of Fe_3O_4 and MWNT in the nanocomposite films. A 1 h period of ultrasonication was used to disperse the desired amount of additive in 99 ml of distilled water, followed by addition of the corresponding amount of Chitosan and 1 ml of acetic acid with subsequent magnetic stirring for 2 h to facilitate dissolution of Chitosan. This was followed by 30 min of ultrasonication. The solution was then degassed for 30 min to remove bubbles, poured onto a glass plate, and heated at 60 °C under vacuum until dry. The dried Chitosan nanocomposite thin films were then carefully removed from the glass plate. The films had an average thickness of 0.04 mm. The samples were denoted as xMWNT/Chitosan, $y$$Fe_3O_4$/Chitosan and $z$$Fe_3O_4$/MWNT/Chitosan, where x and y represents the weight percentages of MWNT and Fe_3O_4 respectively. In the case of Fe_3O_4/MWNT/Chitosan, z equals the sum of MWNT weight percentage(x) and Fe_3O_4 weight percentage(y); all samples have a one–one weight ratio between fillers. Pure Chitosan films were prepared for comparative reasons.

2.3. Characterization

Electrical conductivity of nanocomposites films was measured at room temperature using a ring probe method with a high resistivity meter (MCP-HT 450, Mistubishi). Wide-angle XRD patterns of Fe_3O_4/CNT/Chitosan nanocomposite films were recorded with a Rigaku Rotaflex (RU-200B) X-ray diffractometer using Cu Kα radiation with a Ni filter. The tube current and voltage were 300 mA and 40 kV, respectively, and data from the 2θ angular regions between 0 and 40° were collected. The tensile properties of nanocomposite films were measured at room temperature with a universal test device (Instron 8871). The surface morphology of nanocomposite films was analyzed by field emission scanning electron microscopy (FE-SEM) (LEO SUPRA 55, Carl Zeiss, Germany). The thermal stability of the films was investigated using a TA instrument (SDT Q600) from 30 °C to 900 °C under a nitrogen atmosphere at a heating rate of 10 °C/min. Dynamic mechanical analysis (DMA) of nanocomposites was performed with a dynamic mechanical analyzer (DMA, Q800, TA Company) using tension membrane clamps at a frequency of 1 Hz and a heating rate of 2 °C/min. Raman analysis of nanocomposites was carried out with a Jasco Raman spectrometer equipped with a CCD detector at a wavelength of 532 nm from 100 to 2000 cm^{-1} for samples cut into $5 \times 10 \times 0.04$ mm strips.

3. Results and discussion

3.1. Electrical conductivity of Fe_3O_4/MWNT/Chitosan nanocomposite films

The electrical conductivity was determined using 5 specimens for each sample. Each sample varied according to nanofiller content. The nanofiller content was expressed as a weight percentage (wt%) of the three different fillers, Fe_3O_4, MWNT, and Fe_3O_4/MWNT. Pure Chitosan films exhibited an average conductivity of 1.91×10^{-4} μS/cm. Nanocomposite films using only Fe_3O_4 as filler had conductivity values well below 10^{-3} μS/cm and did not display any tendency or behavior representative of the Fe_3O_4 loading (see Fig. 1). Hence, the use of Fe_3O_4 alone in the nanocomposite film did not have any effect on conductivity.

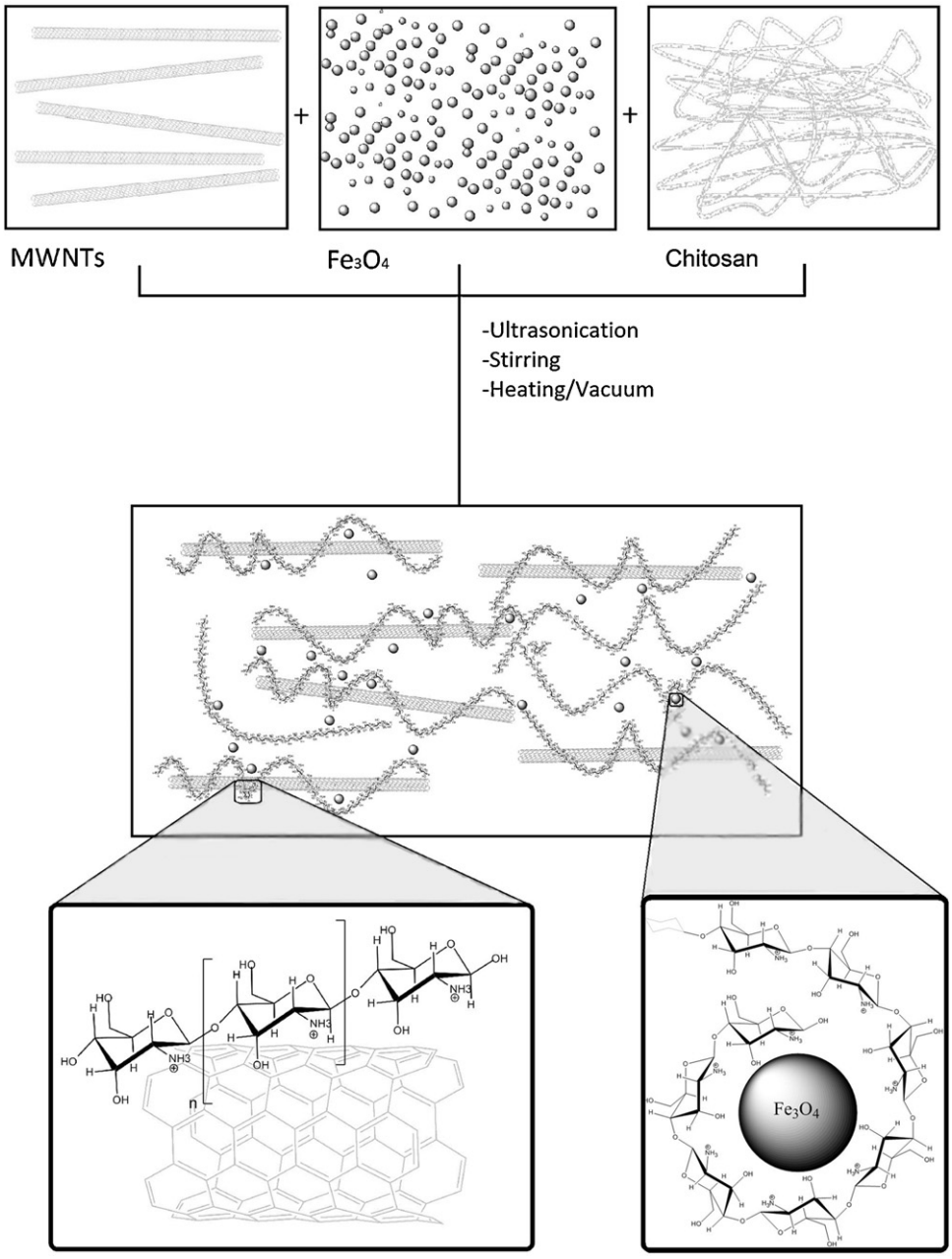

Scheme 1. Preparation of Chitosan nanocomposites.

However, Fe_3O_4 loading did have an effect on the conductivity of the nanocomposite film containing MWNT.

Our previous published results (Marroquin, Kim, Jung, & Rhee, 2012) indicated that the conductivity improved with increasing Fe_3O_4 content, expressed as a weight percentage relative to MWNT content, reaching a maximum at 100% loading with a subsequent decrease from a higher Fe_3O_4 content. Therefore, a 1:1 ratio of Fe_3O_4 to MWNT in the Chitosan nanocomposite film was the optimal loading for conductivity enhancement.

The dependence of Chitosan nanocomposite conductivity on the MWNT and Fe_3O_4/MWNT loading is also shown in Fig. 1. The results clearly indicate that conductivity improved with increased MWNT and Fe_3O_4/MWNT loadings. At low concentrations (0.05–2%), the nanocomposite conductivity gradually increased relative to the nanofiller content. At higher concentrations (5% and 8%), there was a logarithmic increase in conductivity with slight increases of nanofiller loading. This stepwise change in conductivity results from the formation of an interconnected structure of CNTs and can be regarded as the electrical percolation threshold.

The establishment of a highly conductive MWNT/Chitosan film requires a network of effective tube-tube contacts. The quality of such a network is ultimately defined by the nanotube concentration and the relative extent of homogeneous (i.e., well-distributed within the matrix) to heterogeneous distribution (i.e., formation of aggregates). Nanotube dimensions limit the effectiveness of electron tunneling across tube-tube contacts. The dimensions are defined by the critical volume/length ratio and the coating behavior of the polymer, which might insulate the tubes. The homogeneous distribution of MWNT is clearly an important design criterion toward achieving good transfer of electrical charge, as has been demonstrated with two-dimensional polystyrene films (Watts et al., 2001). In those systems, an assumed homogeneous MWNT network was formed via tube-tube bundling and crossing within the polystyrene film matrix, yielding relatively low

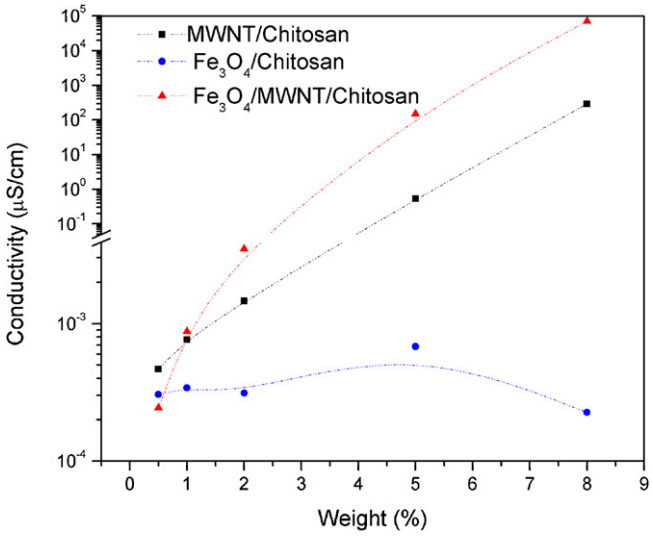

Fig. 1. Conductivity of Chitosan nanocomposites.

resistance (Watts, Hsu, Randall, Kroto, & Walton, 2002). Similar studies on conductive two-dimensional polymer/MWCNT films reported percolation concentrations of 10 wt% for polyvinyl alcohol (Shaffer & Windle, 1999) and 10 wt% for a polyphenylenevinylene polymer (Curran et al., 1998). Furthermore, Fe_3O_4 could facilitate electron transfer between nanotubes while being dispersed in the polymer matrix because the nanocomposite would acquire more conductive channels through interactions between CNT and Fe_3O_4 (0 0 1) surfaces. DFT calculations determined carbon vacancies could form chemical bonds with the Fe_3O_4 (0 0 1) surface, but the binding and electrical conductivity was not significantly improved through the vacancy. However, the calculations determined that TM atoms/clusters could facilitate binding between pristine CNTs and Fe_3O_4 (0 0 1) surfaces through the formation of C—TM and TM—O chemical bonds (Yin et al., 2011). Incorporation of Fe_3O_4 could also result in enhanced crystallinity of the polymer matrix as is further discussed along with additional characterization of the nanocomposites.

3.2. Tensile strength of Chitosan nanocomposites

Tensile tests were performed using the nanocomposites with the highest electrical conductivities, 5 wt% and 8 wt%, to determine the nanocomposite with the best combined conductive and mechanical properties. Fig. 2 compares the mechanical properties of Chitosan, the MWNT/Chitosan and Fe_3O_4/MWNT/Chitosan nanocomposites. The tensile strength was determined to be the maximum stress in the stress–strain curve as shown in Fig. 2a. Fig. 2b shows the tensile strength of the 5% Fe_3O_4/MWNT/Chitosan nanocomposite was 159%, 70%, 64%, and 50% higher than that of Chitosan, 5% MWNT/Chitosan, 8% MWNT/Chitosan, and 8% Fe_3O_4/MWNT/Chitosan nanocomposites, respectively. The elastic modulus was determined by measuring the slope of a linear region of the stress-strain curve (Tang et al., 2009). Similar to the tensile strength results, the elastic modulus improved with the addition of Fe_3O_4 as shown in Fig. 2c. Specifically, the elastic modulus of the 5% Fe_3O_4/MWNT/Chitosan was 179%, 155% and 106% higher than that of Chitosan, 5% MWNT/Chitosan and 8% MWNT/Chitosan nanocomposites, respectively.

Fig. 2a shows tensile stress-strain curves of Chitosan, 5% MWNT/Chitosan and 5% Fe_3O_4/MWNT/Chitosan nanocomposites.

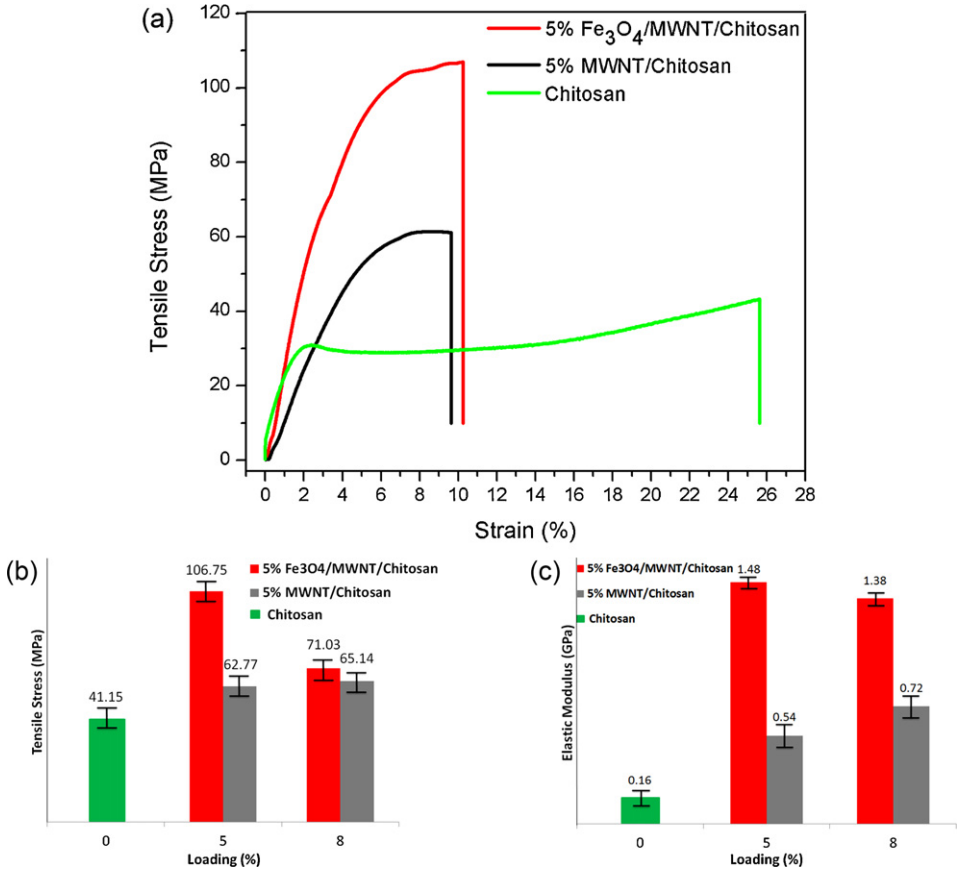

Fig. 2. (a) Tensile strength of the Chitosan nanocomposites. (b) Tensile stress. (c) Elastic modulus.

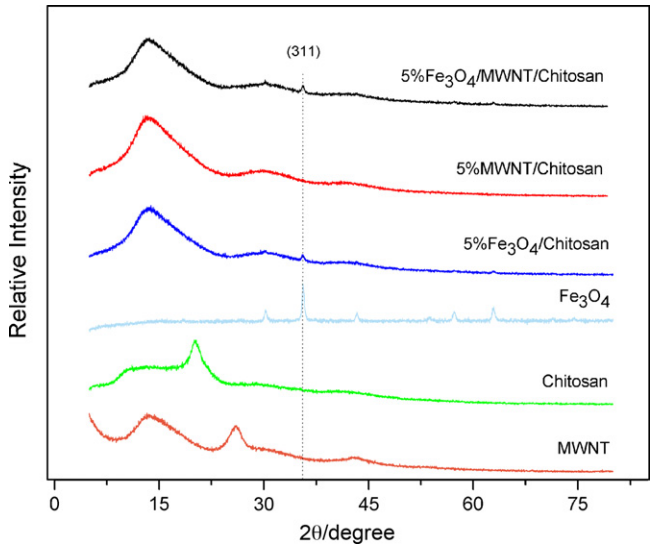

Fig. 3. XRD patterns of Chitosan, MWNT, Fe_3O_4, and Chitosan nanocomposites.

The pure Chitosan specimens presented lower stress and much higher strain values than their nanocomposite counterparts. Furthermore their stress–strain profile presented strain hardening, indicating ductility and semi-crystalline polymer behavior (Kuila et al., 2011). Contrariwise, the MWNT/Chitosan and 5% Fe_3O_4/MWNT/Chitosan nanocomposites did not present strain hardening, stress increased almost linearly with strain in the early stages, with nonlinear behavior occurring before the maximum stress was reached at low strain values.

The tensile strength and modulus of the MWNT/Chitosan nanocomposites were improved by adding Fe_3O_4. The relatively low strain of 5% Fe_3O_4/MWNT/Chitosan and 5% MWNT/Chitosan evidenced brittle tensile behavior, which is characteristic upon addition of nanofillers in polymer nanocomposites (Darder et al., 2003). These results clearly indicate the best combined (conductivity and tensile strength) performance was achieved with a loading of 5% nanofiller.

3.3. X-ray diffraction (XRD)

Diffraction patterns of Chitosan, MWNT, Fe_3O_4, and the nanocomposite films are shown in Fig. 3. The characteristic sharp peak of MWNT at $2\theta = 26^\circ$ representing C (0 0 2) was attributed to the ordered arrangement of concentric cylinders of graphitic carbon (Li et al., 2003) in the nanotube. This crystalline peak disappeared in the nanocomposite samples, which suggests the MWNT were dispersed into the Chitosan matrix (Wang, Shen, Zhang, et al., 2005). XRD patterns for the Fe_3O_4 nanoparticles displayed characteristic peaks ($2\theta = 30.1^\circ$, 35.5°, 43.1°, 53.4°, 57.0°, and 62.6°), which were consistent with those found in the JCPDS database (PDF No. 65-3107). The (3 1 1) peak at $2\theta = 35.5^\circ$ indicates the presence of pure Fe_3O_4 nanoparticles in the Fe_3O_4/Chitosan and Fe_3O_4/MWNT/Chitosan nanocomposites.

For Chitosan, one broad peak was observed at $2\theta = 20^\circ$ (maximum intensity), which corresponded to the characteristic peak of Chitosan chains aligned through intermolecular interactions (Yamaguchi et al., 2001). Ogawa et al. have proposed three forms of Chitosan, noncrystalline, hydrated crystalline, and anhydrous crystalline, with characteristic peaks ranging from 10 to 20° (Ogawa, Hirano, Miyanishi, Yui, & Watanabe, 1984). The peak around $2\theta = 14.2^\circ$ corresponded to the anhydrous crystalline structure of Chitosan (Wang, Shen, Zhang, et al., 2005). This crystalline peak became more pronounced after incorporating the desired amounts of MWNT and Fe_3O_4 into Chitosan. The peak at this angle being a broad peak may indicate the presence of another polymorph, such as the hydrated crystalline structure, which exhibits a peak at $2\theta = 11.7^\circ$. This result suggests an enhanced crystallinity or denser packing in the main chain in comparison with neat Chitosan (Tang et al., 2008) and is consistent with other reports of enhanced crystallinity caused by CNT incorporation (Tang et al., 2009; Wang, Shen, Zhang, et al., 2005; Wang, Shen, Tong, & Liu, 2005).

To measure the relative crystallinity (X_c) of the film, the amorphous areas and crystalline peak areas were measured, and X_c was calculated from diffraction intensity data ($2\theta = 5$-60°) with the following relationship (Tang et al., 2008):

$$X_c = 100 \times \frac{A_c}{(A_c + A_a)}$$

where A_c and A_a are the areas of the crystalline and amorphous regions, respectively. The Chitosan, 5% Fe_3O_4/MWNT/Chitosan and 5% MWNT/Chitosan nanocomposite films exhibited values of $X_c = 24\%$, 77% and 70%, respectively, thus confirming enhanced crystallinity from Fe_3O_4 incorporation. This enchanced crystallinity was reflected in the higher electrical conductivity and tensile strength determined in the previous characterizations.

3.4. Thermogravimetric analysis

TGA curves and the corresponding derivatograms (DTG) of MWNT/Chitosan and Fe_3O_4/MWNT/Chitosan nanocomposites are shown in Fig. 4. There were three major peaks on the DTG curves. The first peak, which appeared around 50–120 °C, can be explained as the evaporation of physically adsorbed and strongly hydrogen bonded water to Chitosan and MWNT (Mansfield, Kar, & Hooker, 2010; Tripathy, Mishra, Yadav, & Behari, 2010; Zawadzki & Kaczmarek, 2010).

The nanocomposites were degraded in two stages; the predominant stage of thermal degradation appeared in the 120–400 °C range during which an approximate 46% drop of nanocomposite mass was observed. This was caused by depolymerization of Chitosan chains through deacetylation and cleavage of glycosidic linkages via dehydration and deamination (Mansfield et al., 2010; Ou et al., 2010; Pawlak & Mucha, 2003; Zawadzki & Kaczmarek, 2010). The decarboxylation of CNT defective sites has also been reported in this temperature range (Fernandes et al., 2010).

The second degradation stage (400–700 °C) consisted of the thermal destruction of the pyranose ring to produce formic, acetic, and butyric acids as well as a series of lower fatty acids (Mansfield et al., 2010; Ou et al., 2008; Ou et al., 2010; Pawlak & Mucha, 2003; Zawadzki & Kaczmarek, 2010). Further degradation occurred for disordered carbon derived from thermal oxidation of CNTs and Chitosan (Mansfield et al., 2010). For the Fe_3O_4 containing nanocomposite, a barely noticeable additional third degradation stage could be suggested at 750–800 °C, which would correspond to the reduction of Fe_3O_4 by reaction with residual carbon (Rudolph, Erler, & Peuker, 2012).

It is generally accepted that reliable degradation temperature and kinetic parameters, such as polymer degradation temperature (PDT), maximum degradation temperature (T_{max}), integral procedure decomposition temperature (IPDT) and activation energy (E_a), can be used to assess the lifetime of a material (Doyle, 1961; Zohuriaan & Shokrolahi, 2004). The IPDT proposed by Doyle (Doyle, 1961) is calculated as follows:

$$\text{IPDT}\,(^\circ\text{C}) = A^* K^* (T_f - T_i) + T_i$$

$$A^* = \frac{S_1 + S_2}{S_1 + S_2 + S_3}$$

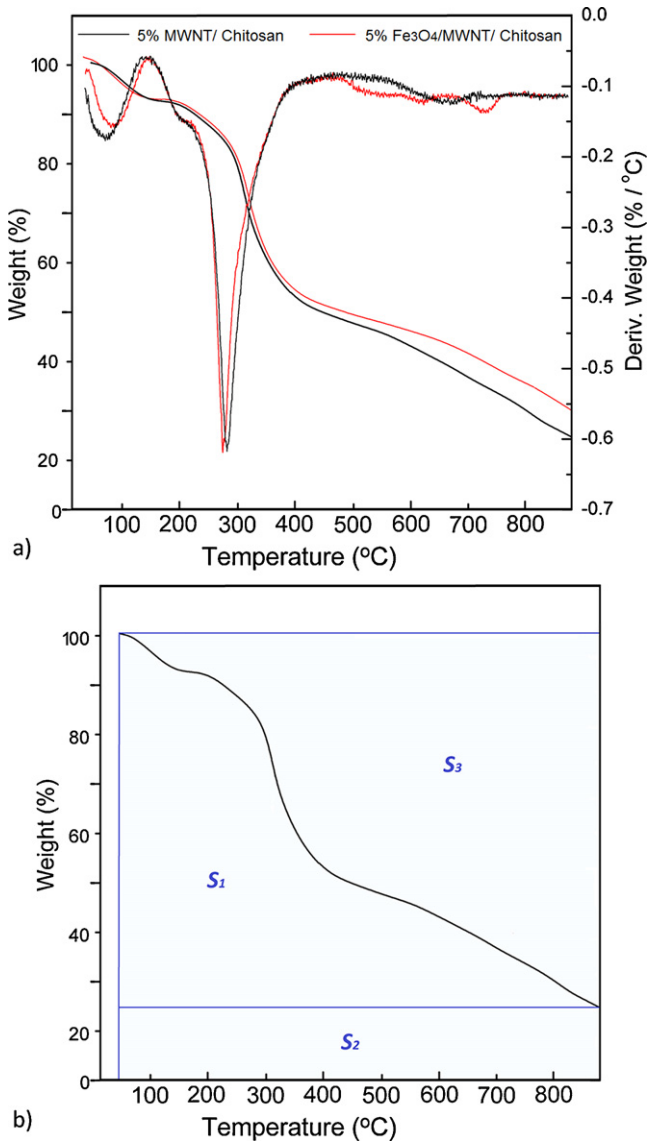

Fig. 4. (a) Thermograms of Chitosan nanocomposites. (b) Schematic representation of S_1, S_2 and S_3 for A^* and K^*.

$$K^* = \frac{S_1 + S_2}{S_1}$$

where A^* is the area ratio of the total experimental curve defined by the total TGA thermogram, K^* is the coefficient of A^*, T_i is the initial experimental temperature, and T_f is the final experimental temperature. Fig. 4b shows a representation of S_1, S_2, and S_3 for calculating A^* and K^*.

The IPDT values for MWNT/Chitosan and Fe_3O_4/MWNT/Chitosan, shown in Table 1, indicate higher thermal stability due to Fe_3O_4 incorporation. Both nanocomposites showed enhanced thermal stability compared to regular Chitosan; the reported IPDT value for Chitosan (Zohuriaan & Shokrolahi, 2004) is 417 °C.

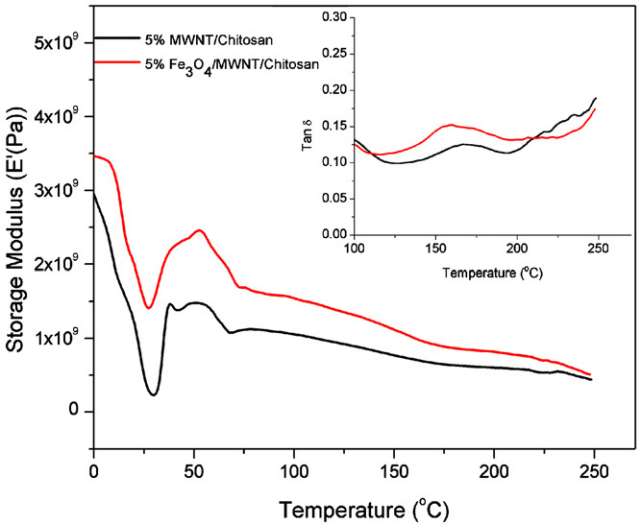

Fig. 5. Dynamical mechanical analysis of Chitosan nanocomposites.

The apparent activation energy, E_a, for the thermal degradation stages of nanocomposites was calculated from the TGA thermogram using Broido's (Broido, 1969) equation:

$$\ln[-\ln(1-\alpha)] = -\frac{E_{a,dec}}{RT} + \text{const.}$$

$$\alpha = \frac{W_0 - W_t}{W_0 - W_\infty}$$

where α is the extent of decomposition, W_t, W_0, and W_∞ are the actual, initial, and final masses of the sample, respectively, R is the universal gas constant, T is the absolute temperature, and $E_{a,dec}$ is the activation energy for thermal decomposition. The apparent activation energy for the major decomposition stage was obtained by plotting $\ln[-\ln(1-\alpha)]$ versus $1/T$. Analysis of the thermal degradation kinetics showed that Fe_3O_4 addition increased the activation energy for the main degradation stage in the nanocomposites. These results are summarized in Table 1.

The overall higher thermal stability of Fe_3O_4 containing nanocomposites indicates incorporation of these nanoparticles into the Chitosan matrix greatly affects the activation energy of the first and major stages of decomposition and suggests a hindrance of depolymerization of the main Chitosan chains through chemical interactions.

3.5. Dynamic mechanical analysis (DMA)

Variations of storage modulus (E') and $\tan\delta$ of the 5% MWNT/Chitosan and 5% Fe_3O_4/MWNT/Chitosan nanocomposites are shown in Fig. 5. The 5% Fe_3O_4/MWNT/Chitosan nanocomposite had a higher E' than the 5% MWNT/Chitosan nanocomposite (Fig. 5), which suggests that the interactions between the Chitosan matrix, MWNT, and Fe_3O_4 are stronger and allow a more efficient load transfer (Tang et al., 2009). The enhanced storage modulus

Table 1
Thermal parameters of the Chitosan nanocomposites.

Sample	PDT (°C)	A^*	K^*	T_{max} (°C)	IPDT (°C)	$E^*_{a,dec}$ (kJ/mol)
MWNT/Chitosan	125.9	0.48	1.16	275	501.2	105.0
Fe_3O_4/MWNT/Chitosan	133.7	0.50	1.26	271	568.5	117.8

$E^*_{a,dec}$: Activation energy for main decomposition stage according to the Broido method.

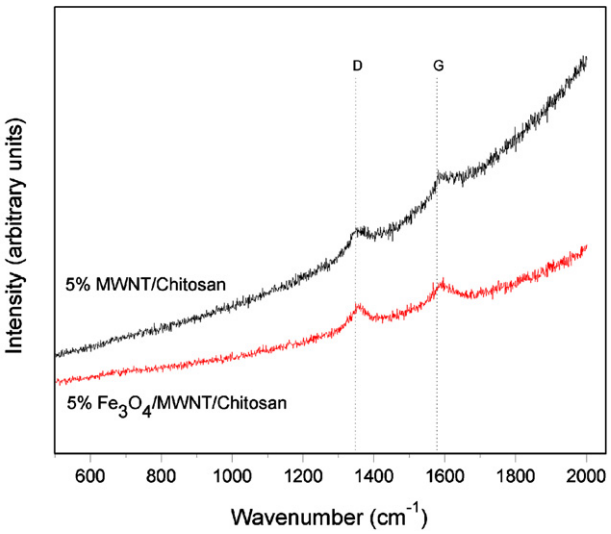

Fig. 6. Raman spectra of Chitosan nanocomposites.

also indicates improved dispersion of MWNT in the nanocomposite (Kabiri et al., 2011).

The glass transition temperature (T_g) of samples can be provided from the tanδ curves (Fig. 5 inset). The T_g for 5% MWNT/Chitosan and 5% Fe_3O_4/MWNT/Chitosan nanocomposites was determined to be 166 and 161 °C, respectively. In view that the T_g of the nanocomposites shift to lower temperatures and the tensile moduli of the nanocomposites are increased with loadings of Fe_3O_4 (Fig. 2), these results appear to contradict the general phenomenon observed for many filled polymeric systems, in which higher moduli correlate with higher T_gs. This observed behavior is termed antiplasticization. Reported studies (Jackson & Caldwell, 1967a) define antiplasticization as a simultaneous decrease in T_g with increased mechanical stiffening and embrittlement caused by the addition of particular substances to polymers. Tensile results (Fig. 2) showed that the addition of Fe_3O_4 induce the embrittlement of the matrix (i.e., a decreasing tendency of ultimate elongation). These results are also in good agreement with previous works using nanosized silica, silver, and aluminum that have shown antiplasticization leading to embrittlement of polymers (Sun, Zhang, Moon, & Wong, 2004). The mechanism of antiplasticization is perhaps a combination of several factors: tight filling of the free volume of the polymer molecules, interaction between the polar groups of the polymer and of the antiplasticizer, a physical stiffening action due to the presence of rigid small molecules adjacent to the polar groups of the polymer and consequently the restriction of local, noncooperative in-chain molecular motions. (Jackson & Caldwell, 1967b). Because the most flexible portions of a rigid condensation polymer are its polar groups the interaction of these groups with stiff and polar antiplasticizer molecules should reduce the flexibility. It can be reasonably concluded that the mechanism of the tight filling of the free volume of a polymer matrix and physical stiffening due to the presence of rigid Fe_3O_4 nanoparticles may be the sole cause of the antiplasticization in this system. A similar observation of the lowering of T_g in ultrathin polymer films in the presence of nanosized materials (<100 nm) has been termed nanoconfinement of polymer properties by different researchers (Ghosh et al., 2007).

The tan δ peak height was enhanced in the 5% Fe_3O_4/MWNT/Chitosan nanocomposite compared with the 5% MWNT/Chitosan sample. The magnitude of the tan δ peak is related to the damping capability, or vibrational energy dissipation, which reflects the toughness or stiffness of a material at the relaxation temperature (Kuila et al., 2011). These results further corroborate the thermal study observations.

3.6. Raman spectroscopy

Raman spectroscopy was used to investigate interfacial interactions between the Chitosan matrix, Fe_3O_4 nanoparticles, and MWNT. Fig. 6 shows high frequency Raman spectra for Fe_3O_4/MWNT/Chitosan and MWNT/Chitosan nanocomposites with 5% addition of nanofillers. The spectra of the MWNT/Chitosan nanocomposite displayed two characteristic peaks: 1350 cm^{-1},

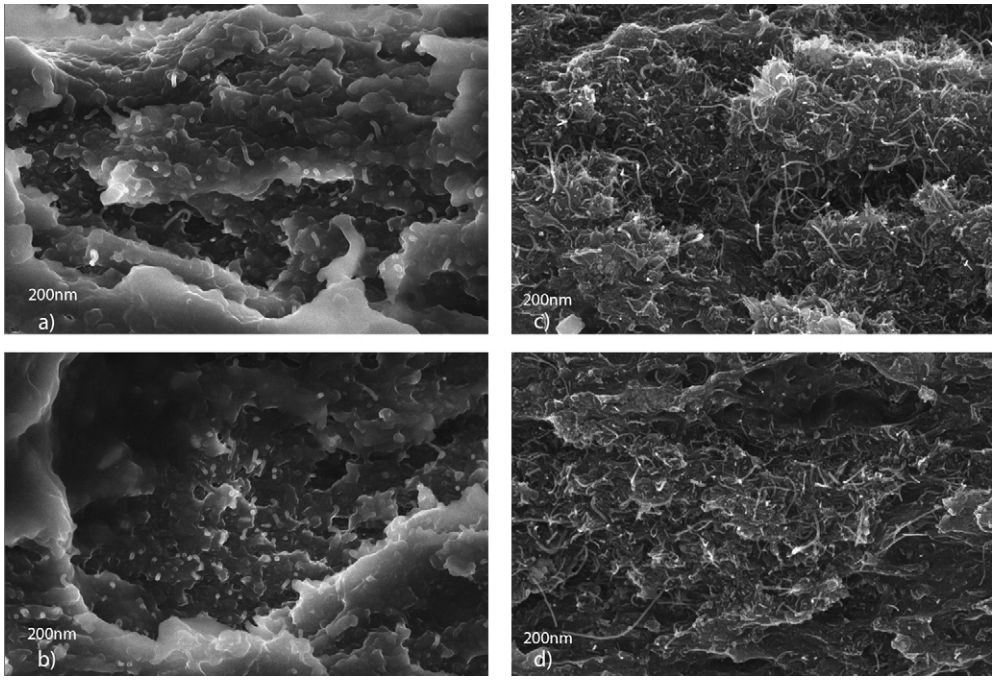

Fig. 7. FESEM images of fracture surfaces of Chitosan nanocomposites. FESEM images of 5% Fe_3O_4/MWNT/Chitosan (a) to (b) and 5% MWNT/Chitosan nanocomposites (c) to (d).

corresponding to the D band and derived from disordered graphite structures, and approximately 1580 cm^{-1}, assigned to the G band and associated with tangential C—C bond stretching motions originating from the E_{2g2} mode at 1580 cm^{-1} in graphite (Dresselhaus, Dresselhaus, Jorio, Souza, & Saito, 2002; McNally et al., 2005). Upon addition of Fe_3O_4, the maximum in the G band peak was blue shifted by 16 cm^{-1}. This observation can be rationalized as disentanglement of MWNT and their subsequent dispersion into the Chitosan matrix from polymer penetration into the MWNT bundles during the nanocomposite preparation. Thus, interactions between the Fe_3O_4, Chitosan, and MWNT were responsible for increasing the energy necessary for vibrations and shifting the Raman band to a higher frequency. These results indicate there are attractive interactions between the Chitosan chains, MWNT, and Fe_3O_4 nanoparticles. A similar up-shift of the G band has been reported for MWNT reinforced polyethylene nanocomposites (McNally et al., 2005); in the case of SWCNTs, an up-shift of the G band has also been reported, albeit much smaller than 16 cm^{-1}, for epoxy resins (Hadjiev, Iliev, Arepalli, Nikolaev, & Files, 2001; Puglia, Valentini, & Kenny, 2003) and polystyrene (Valentini, Biagiotti, Kenny, & Santucci, 2003).

3.7. Field emission scanning electron microscopy (FESEM)

Morphological characterization of nanocomposite films was conducted using FESEM analysis. Fig. 7 shows typical fracture surfaces of the Chitosan nanocomposites. The fractured surface of the Fe_3O_4/MWNT/Chitosan nanocomposites exhibited improved dispersion of MWNT characterized by the presence of individual isolated nanotubes within the Chitosan matrix (Fig. 7(a) and (b)). A uniform distribution of MWNT was observed, with the ends of broken nanotubes on the fractured surface. The observation that most of the MWNT were broken rather than pulled out from the matrix indicates a strong interfacial adhesion between the MWNT and Chitosan matrix. Good dispersion and interfacial stress transfer are important factors for preparing reinforced nanocomposites, which results in a more uniform stress distribution and minimizes the presence of stress concentration centers (Coleman, Khan, & Gun'ko, 2006). These FESEM images confirmed the previous observations from the XRD, Raman, and TG analyses. In contrast, the MWNT/Chitosan nanocomposites (Fig. 7(c) and (d)) were comprised of MWNT intertwined within the Chitosan matrix generating large aggregation clusters. Additionally, some long nanotubes were observed on the fracture surface indicating a pulling mechanism upon tension and suggest a weaker interfacial adhesion with the Chitosan matrix. These factors were reflected in the lower mechanical properties observed with this nanocomposite.

4. Conclusion

A hitherto unreported high-performance Fe_3O_4/MWNT/Chitosan nanocomposite film was prepared by a simple eco-friendly solution evaporation method, which can be used for a broad range of biomaterial applications such as biosensing and bioenergetics. Although the use of MWNT on Chitosan has already been studied, the combined use of Fe_3O_4 and MWNTs provide a significant synergistic effect regarding mechanical properties, relative crystallinity, thermal stability and electrical conductivity. Hence, the Fe_3O_4/MWNT/Chitosan nanocomposites were far superior to neat Chitosan and the MWNT/Chitosan nanocomposites. The 5% Fe_3O_4/MWNT/Chitosan nanocomposites exhibited an increase in tensile modulus compared to those of neat Chitosan and 5% MWNT/Chitosan nanocomposites by 179% and 155% respectively. Conductivity was improved from 1.91×10^{-8} S/m for Chitosan, to 5.34×10^{-5} S/m for 5% MWNT/Chitosan and 1.49×10^{-2} S/m for 5% Fe_3O_4/MWNT/Chitosan nanocomposites. Thermal stability (i.e., IPDT) was enhanced from 417 °C to 501 °C and 568 °C for Chitosan, 5% MWNT/Chitosan and 5% Fe_3O_4/MWNT/Chitosan respectively. Fe_3O_4 acted as an antiplasticizer agent leading to higher crystallinity as well as restricted mobility of Chitosan chain segments, thus, further improving the mechanical properties of the nanocomposite films. To the best of our knowledge, this is the first study reporting that Chitosan nanocomposites films could simultaneously have enhanced mechanical properties, thermal stability and electrical conductivity by using Fe_3O_4 and MWNT. The introduction of these two functional additives with different properties and structure for the improvement of materials properties may be applicable to other materials.

Acknowledgement

This work was supported by Basic Science Research Program through the National Research Foundation of Korea (NRF) funded by the Ministry of Education, Science and Technology (2010-0023106). The authors would like to thank Dr. Mithilesh Yadav, who works as a Research Professor in the Nanocomposite Laboratory, Kyung Hee University, South Korea; for his suggestions and fruitful comments during the realization of this work.

References

Ajayan, P. M., Schadler, L. S., Giannaris, C., & Rubio, A. (2000). Single-walled carbon nanotube–polymer composites: Strength and weakness. *Advanced Materials*, *12*(10), 750–753.

Broido, A. (1969). A simple, sensitive graphical method of treating thermogravimetric analysis data. *Journal of Polymer Science Part A-2: Polymer Physics*, *7*, 1761–1773.

Cai, X., Tong, H., Shen, X. Y., Chen, W. X., Yan, J., & Hu, J. M. (2009). Preparation and characterization of homogeneous chitosan–polylactic acid/hydroxyapatite nanocomposite for bone tissue engineering and evaluation of its mechanical properties. *Acta Biomaterialia*, *5*(7), 2693–2703.

Coleman, J., Khan, U., & Gun'ko, Y. (2006). Mechanical reinforcement of polymers using carbon nanotubes. *Advanced Materials*, *18*, 689–706.

Curran, S. A., Ajayan, P. M., Blau, W. J., Carroll, D. L., Coleman, J. N., Dalton, A. B., et al. (1998). A composite from poly(m-phenylenevinylene-co-2,5-dioctoxy-p-phenylenevinylene) and carbon nanotubes. A novel material for molecular optoelectronics. *Advanced Materials*, *10*(14), 1091–1093.

Darder, M., Colilla, M., & Ruiz-Hitzky, E. (2003). Biopolymer–clay nanocomposites based on chitosan intercalated in montmorillonite. *Chemistry of Materials*, *15*(20), 3774–3780.

Ding, J., Gao, Q., Li, X., Huang, W., Shi, Z., & Feng, Y. (2011). Magnetic solid-phase extraction based on magnetic carbon nanotube for the determination of estrogens in milk. *Journal of Separation Science*, *34*(18), 2498–2504.

Doyle, C. D. (1961). Estimating thermal stability of experimental polymers by empirical thermogravimetric analysis. *Analytical Chemistry*, *33*(1), 77–79.

Dresselhaus, G., Dresselhaus, M. S., Jorio, A., Souza, A., & Saito, R. (2002). Raman spectroscopy on isolated single wall carbon nanotubes. *Carbon*, *40*(12), 2043–2061.

Fernandes, S. C. M., Freire, C. S. R., Silvestre, A. J. D., Pascoal Neto, C., Gandini, A., Berglund, L. A., et al. (2010). Transparent chitosan films reinforced with a high content of nanofibrillated cellulose. *Carbohydrate Polymers*, *81*(2), 394–401.

Georgakilas, V., Gournis, D., Tzitzios, V., Pasquato, L., Guldie, D. M., & Prato, M. (2007). Decorating carbon nanotubes with metal or semiconductor nanoparticles. *Journal of Materials Chemistry*, *17*, 2679–2694.

Ghosh, A., Sciamanna, S. F., Dahl, E., Liu, S., Carlson, R. M. K., & Schiraldi, D. A. (2007). Effect of nanoscale diamondoid on the thermomechanical and morphological behaviors of polypropylene and polycarbonate. *Journal of Applied Polymer Science Part B: Polymer Physics*, *42*(9), 1077–1089.

Hadjiev, V. G., Iliev, M. N., Arepalli, S., Nikolaev, P., & Files, B. S. (2001). Raman scattering test of single-wall carbon nanotube composites. *Applied Physics Letters*, *78*(21), 3193–3195.

Jackson, W. J., & Caldwell, J. R. (1967a). Antiplasticization. II. Characteristics of antiplasticizers. *Journal of Applied Polymer Science*, *11*(2), 211–226.

Jackson, W. J., & Caldwell, J. R. (1967b). Antiplasticization. III. Characteristics and properties of antiplasticizers. *Journal of Applied Polymer Science*, *11*(2), 227–244.

Kabiri, K., Hesarian, S., Zohuriaan-Mehr, M., Jamshidi, H., Boohendi, M., Pourheravi, S., et al. (2011). Superabsorbent polymer composites: Does clay always improve properties? *Journal of Materials Science*, *46*, 6718–6725.

Kaushik, A., Khan, R., Solanki, P. R., Pandey, P., Alam, J., Ahmad, S., et al. (2008). Iron oxide nanoparticles–chitosan composite based glucose biosensor. *Biosensors and Bioelectronics*, *24*(4), 676–683.

Kuila, T., Bose, S., Khanra, P., Kim, N. H., Rhee, K. Y., & Lee, J. H. (2011). Characterization and properties of in situ emulsion polymerized

poly(methylmethacrylate)/graphene nanocomposites. *Composites: Part A*, *42*, 1856–1861.
Kwon, J., & Kim, H. (2005). Comparison of the properties of waterborne polyurethane/multiwalled carbon nanotube and acid-treated multiwalled carbon nanotube composites prepared by in situ polymerization. *Journal of Polymer Science, Part A: Polymer Chemistry*, *43*(17), 3973–3985.
Landi, B. J., Raffaelle, R. P., Heben, M. J., Alleman, J. L., VanDerveer, W., & Gennett, T. (2002). Single wall carbon nanotube–nafion composite actuators. *Nano Letters*, *2*(11), 1329–1332.
Li, G., Jiang, Y., Huang, K., Ding, P., & Chen, J. (2008). Preparation and properties of magnetic Fe_3O_4–chitosan nanoparticles. *Journal of Alloys and Compounds*, *466*, 451–456.
Li, N., Huang, Y., Du, F., He, X., Lin, X., Gao, H., et al. (2006). Electromagnetic interference (EMI) shielding of single-walled carbon nanotube epoxy composites. *Nano Letters*, *6*(6), 1141–1145.
Li, W., Liang, C., Zhou, W., Quip, J., Zhou, Z., Sun, G., et al. (2003). Preparation and characterization of multiwalled carbon nanotube-supported platinum for cathode catalysts of direct methanol fuel cells. *Journal of Physical Chemistry B*, *107*, 6292–6299.
Liu, Y., Qu, X., Guo, H., Chen, H., Liu, B., & Dong, S. (2006). Facile preparation of amperometric lactase biosensor with multifunction based on the matrix of carbon nanotubes–chitosan composite. *Biosensors and Bioelectronics*, *21*(12), 2195–2201.
Liu, Y., Tang, J., Chen, X., & Xin, J. H. (2005). Decoration of carbon nanotubes with chitosan. *Carbon*, *43*(15), 3178–3180.
Luo, Y., Yu, Q., Yuan, B., & Feng, Y. (2012). Fast microextraction of phthalate acid esters from beverage, environmental water and perfume samples by magnetic multi-walled carbon nanotubes. *Talanta*, *90*, 123–131.
Mansfield, E., Kar, A., & Hooker, S. A. (2010). Applications of TGA in quality control of SWCNTs. *Analytical and Bioanalytical Chemistry, 396*(3), 1071–1077.
Marroquin, J., Kim, H. J., Jung, D. H., & Rhee, K. Y. (2012). Effect of Fe_3O_4 loading on the conductivities of carbon nanotube/chitosan composite films. *Carbon Letters*, *13*(2), 126–129.
McNally, T., Petra Potschke, P., Halley, P., Murphy, M., Martin, D., Bell, S., et al. (2005). Polyethylene multiwalled carbon nanotube composites. *Polymer*, *46*, 8222–8232.
Miao, Y., & Tan, S. N. (2000). Amperometric hydrogen peroxide biosensor based on immobilization of peroxidase in chitosan matrix crosslinked with glutaraldehyde. *Analyst*, *125*(9), 1591–1594.
Muzzarelli, R. A. A., Boudrant, J., Meyer, D., Manno, N., DeMarchis, M., & Paoletti MG. (2012). Current views on fungal chitin/chitosan, human chitinases, food preservation, glucans, pectins and inulin: A tribute to Henri Braconnot, precursor of the carbohydrate polymers science, on the chitin bicentennial. *Carbohydrate Polymers*, *87*, 995–1012.
Muzzarelli, R. A. A., Greco, F., Busilacchi, A., Sollazzo, V., & Gigante, A. (2012). Chitosan, hyaluronan and chondroitin sulfate in tissue engineering for cartilage regeneration: A review. *Carbohydrate Polymers*, *89*, 723–739.
Ogawa, K., Hirano, S., Miyanishi, T., Yui, T., & Watanabe, T. (1984). A new polymorph of chitosan. *Macromolecules*, *17*(4), 973–975.
Ou, C. Y., Li, S. D., Li, C. P., Zhang, C. H., Yang, L., & Chen, C. P. (2008). Effect of cupric ion on thermal degradation of chitosan. *Journal of Applied Polymer Science*, *109*, 957–962.
Ou, C. Y., Zhang, C. H., Li, S. D., Yang, L., Dong, J. J., Mo, X. L., et al. (2010). Thermal degradation kinetics of chitosan–cobalt complex as studied by thermogravimetric analysis. *Carbohydrate Polymers*, *82*(4), 1284–1289.
Pawlak, A., & Mucha, M. (2003). Thermogravimetric and FTIR studies of chitosan blends. *Thermochimica Acta*, *396*, 153–166.
Puglia, D., Valentini, L., & Kenny, J. M. (2003). Analysis of the cure reaction of carbon nanotubes/epoxy resin composites through thermal analysis and Raman spectroscopy. *Journal of Applied Polymer Science*, *88*(2), 452–458.
Qian, L., & Yang, X. (2006). Composite film of carbon nanotubes and chitosan for preparation of amperometric hydrogen peroxide biosensor. *Talanta*, *68*(3), 721–727.
Qua, S., Wang, J., Kong, J., Yang, P., & Chen, G. (2007). Magnetic loading of carbon nanotube/nano-Fe_3O_4 composite for electrochemical sensing. *Talanta*, *71*, 1096–1102.
Rudolph, M., Erler, J., & Peuker, U. A. (2012). A TGA-FTIR perspective of fatty acid adsorbed on magnetite nanoparticles-decomposition steps and magnetite reduction. *Colloids and Surfaces A: Physicochemical and Engineering Aspects*, *397*, 16–23.
Shaffer, M. S. P, & Windle, A. H. (1999). Fabrication and characterization of carbon nanotube/poly(vinyl alcohol) composites. *Advanced Materials*, *11*(11), 937–941.
Sun, Y., Zhang, Z., Moon, K.-S., & Wong, C. P. (2004). Glass transition and relaxation behavior of epoxy nanocomposites. *Journal of Applied Polymer Science Part B: Polymer Physics*, *42*(21), 3849–3858.
Tang, C., Chen, N., Zhang, Q., Wang, K., Fu, Q., & Zhang, X. (2009). Preparation and properties of chitosan nanocomposites with nanofillers of different dimensions. *Polymer Degradation and Stability*, *94*, 124–131.
Tang, C., Xiang, L., Su, J., Wang, K., Yang, C., Zhang, Q., et al. (2008). Largely improved tensile properties of chitosan film via unique synergistic reinforcing effect of carbon nanotube and clay. *Journal of Physical Chemistry B*, *112*(13), 3876–3881.
Tkac, J., Whittaker, J. W., & Ruzgas, T. (2007). The use of single walled carbon nanotubes dispersed in a chitosan matrix for preparation of a galactose biosensor. *Biosensors and Bioelectronics*, *22*(8), 1820–1824.
Tripathy, J., Mishra, D. K., Yadav, M., & Behari, K. (2010). Synthesis, characterization and applications of graft copolymer (Chitosan-g-N,N-dimethylacrylamide). *Carbohydrate Polymers*, *79*(1), 40–46.
Valentini, L., Biagiotti, J., Kenny, J. M., & Santucci, S. (2003). Load transfer and deformation mechanisms in carbon nanotube–polystyrene composites. *Composite Science and Technology*, *63*(8), 1149–1153.
Venkatesan, J., & Kim, S. (2010). Chitosan composites for bone tissue engineering. *Marine Drugs*, *8*, 2252–2266.
Wang, S., Shen, L., Zhang, W., & Tong, Y. (2005). Preparation and mechanical properties of chitosan/carbon nanotubes composites. *Biomacromolecules*, *6*, 3067–3072.
Wang, S. F., Shen, L., Tong, Y. J., & Liu, T. X. (2005). Biopolymer chitosan/montmorillonite nanocomposites: Preparation and characterization. *Polymer Degradation and Stability*, *90*, 123–131.
Watts, P. C. P., Hsu, W. K., Chen, G. Z., Fray, D. J., Kroto, H. W., & Walton, D. R. M. (2001). A low resistance boron-doped carbon nanotube–polystyrene composite. *Journal of Materials Chemistry*, *11*(10), 2482–2488.
Watts, P. C. P., Hsu, W. K., Randall, D. P., Kroto, H. W., & Walton, D. R. M. (2002). Non-linear current-voltage characteristics of electrically conducting carbon nanotube–polystyrene composites. *Physical Chemistry Chemical Physics*, *4*(22), 5655–5662.
Wescott, J. T., Kung, P., & Maiti, A. (2007). Conductivity of carbon nanotube composites. *Applied Physics Letters*, *90*(3), 33116–33119.
Xu, C., Cai, H., He, P., & Fang, Y. (2001). Electrochemical detection of sequence-specific DNA using a DNA probe labeled with aminoferrocene and chitosan modified electrode immobilized with ssDNA. *Analyst*, *126*(1), 62–65.
Yamaguchi, I., Tokuchi, K., Fukuzaki, H., Koyama, Y., Takakuda, K., Monma, H., et al. (2001). Preparation and microstructure analysis of chitosan/hydroxyapatite nanocomposites. *Journal of Biomedical Materials Research*, *55*, 20–27.
Yao, S., Yuan, J., Dang, Z., & Bai, J. (2010). High dielectric performance of three-component nanocomposites induced by a synergetic effect. *Materials Letters*, *64*(24), 2682–2684.
Yin, W. J., Wei, S. H., Ban, C., Wu, Z., Al-Jassim, M., & Yan, Y. (2011). Origin of bonding between the SWCNT and the Fe_3O_4(0 0 1) surface and the enhanced electrical conductivity. *Journal of Physical Chemistry Letters*, *2*(22), 2853–2858.
Yu, C., Gou, L., Zhou, X., Bao, N., & Gu, H. (2011). Chitosan–Fe_3O_4 nanocomposite based electrochemical sensors for the determination of bisphenol A. *Electrochimica Acta*, *56*, 9056–9063.
Zawadzki, J., & Kaczmarek, H. (2010). Thermal treatment of chitosan in various conditions. *Carbohydrate Polymers*, *80*(2), 394–400.
Zhang, M., Smith, A., & Gorski, W. (2004). Carbon nanotube–chitosan system for electrochemical sensing based on dehydrogenase enzymes. *Analytical Chemistry*, *76*(17), 5045–5050.
Zhao, Q., Wei, F., Luo, Y., Ding, J., Xiao, N., & Feng, Y. (2011). Rapid magnetic solid-phase extraction based on magnetic multiwalled carbon nanotubes for the determination of polycyclic aromatic hydrocarbons in edible oils. *Journal of Agricultural and Food Chemistry*, *59*(24), 12794–12800.
Zhu, A., Yuan, L., & Liao, T. (2008). Suspension of Fe_3O_4 nanoparticles stabilized by chitosan and o-carboxymethylchitosan. *International Journal of Pharmaceutics*, *350*(1–2), 361–368.
Zohuriaan, M. J., & Shokrolahi, F. (2004). Thermal studies on natural and modified gums. *Polymer Testing*, *23*(5), 575–579.